Palaeogeography, Palaeoclimatology, Palaeoecology 438 (2015) 245–255

Contents lists available at ScienceDirect

Palaeogeography, Palaeoclimatology, Palaeoecology

journal homepage: www.elsevier.com/locate/palaeo

Ecological and biogeochemical change in an early Paleogene peat-forming environment: Linking biomarkers and palynology

Gordon N. Inglis [a,b,*], Margaret E. Collinson [c], Walter Riegel [d,e], Volker Wilde [e], Brittany E. Robson [c], Olaf K. Lenz [f], Richard D. Pancost [a,b]

[a] Organic Geochemistry Unit, School of Chemistry, University of Bristol, Cantock's Close, Bristol BS8 1TS, UK
[b] Cabot Institute, University of Bristol, Bristol BS8 1UJ, UK
[c] Department of Earth Sciences, Royal Holloway University of London, Egham, Surrey TW20 0EX, UK
[d] Geowissenschaftliches Zentrum Göttingen, Geobiologie, Goldschmidtstrasse 3, D-37077 Göttingen, Germany
[e] Senckenberg Forschungsinstitut und Naturmuseum, Senckenberganlage 25, D-60325 Frankfurt am Main, Germany
[f] TU Darmstadt, Institut für Angewandte Geowissenschaften, Angewandte Sedimentgeologie, Schnittspahnstrasse 9, Germany

ARTICLE INFO

Article history:
Received 28 January 2015
Received in revised form 27 July 2015
Accepted 1 August 2015
Available online 8 August 2015

Editor: T. Correge

Keywords:
Paleocene
Eocene
bryophyte
Sphagnum bog

ABSTRACT

Sphagnum moss is the dominant plant type in modern boreal and (sub)arctic ombrotrophic bogs and is of particular interest due to its sensitivity to climate and its important role in wetland biogeochemistry. Here we reconstruct the occurrence of *Sphagnum* moss – and associated biogeochemical change – within a thermally immature, early Paleogene (~55 Ma) lignite from Schöningen, NW Germany using a high-resolution, multi-proxy approach. Changes in the abundance of *Sphagnum*-type spores and the C_{23}/C_{31} *n*-alkane ratio indicate the expansion of *Sphagnum* moss within the top of the lignite seam. This *Sphagnum* moss expansion is associated with the development of waterlogged conditions, analogous to what has been observed within modern ombrotrophic bogs. The similarity between biomarkers and palynology also indicates that the C_{23}/C_{31} *n*-alkane ratio may be a reliable chemotaxonomic indicator for *Sphagnum* during the early Paleogene. The $\delta^{13}C$ value of bacterial hopanes and mid-chain *n*-alkanes indicates that a rise in water table is not associated with a substantial increase in aerobic methanotrophy. The absence of very low $\delta^{13}C$ values within the top of the seam could reflect either less methanogenesis or less efficient methane oxidation under waterlogged sulphate-rich conditions.

1. Introduction

The early Paleogene (66–34 Ma) is characterised by high atmospheric carbon dioxide (pCO_2) concentrations (Pearson and Palmer, 2000; Pagani et al., 2005; Lowenstein and Demicco, 2006; Pearson et al., 2009), high sea surface temperatures (SST) (Pearson et al., 2007; Bijl et al., 2009; Hollis et al., 2012), high land temperatures (Huber and Caballero, 2011; Pancost et al., 2013) and intensification of the hydrological cycle (Pierrehumbert, 2002; Pagani et al., 2006; Krishnan et al., 2014). As a result, early Paleogene wetland environments may have been up to ~3 times more abundant than today (Sloan et al., 1992; DeConto et al., 2012).

Modern wetlands are the largest natural source of atmospheric methane (CH_4) with estimates ranging between 80 and 280 Tg CH_4 yr^{-1} (Bridgham et al., 2013). As a result, the ecology and biogeochemistry of wetlands are increasingly recognised as central to understanding Paleogene biogeochemical feedbacks. Although there are no proxy methods for reconstructing ancient CH_4 emissions, the carbon isotope value of bacterial hopanes has been used to infer relative changes in terrestrial methane cycling (e.g., Pancost et al., 2007). For example, a decrease in the carbon isotope value of bacterial hopanes during the onset of the Paleocene-Eocene Thermal Maximum (PETM; ~56 Ma) indicates enhanced CH_4 production within an ancient peat-forming environment (Pancost et al., 2007). Over longer timescales, modelling studies suggest a ~6- to 7-fold increase in wetland CH_4 emissions during the early Paleogene (Beerling et al., 2011). Enhanced CH_4 emissions and changes in other biogenic trace gases (i.e., N_2O and O_3) may have acted to increase global temperature by 2.7 °C during the early Paleogene (Beerling et al., 2011) and could have been an important mechanism for maintaining high-latitude warmth (Sloan et al., 1992).

A particularly important topic of interest in palaeoclimate investigations has been tracing the occurrence and distribution of *Sphagnum* moss in wetland environments. *Sphagnum* moss is the dominant plant type in modern ombrotrophic bogs (Clymo, 1984) and plays an important role in terrestrial methane cycling (Raghoebarsing et al., 2005; Kip et al., 2010). Under anoxic, waterlogged conditions, anaerobic degradation of *Sphagnum* produces significant quantities of CH_4 that contribute to the total atmospheric CH_4 flux (Clymo, 1984). However, *Sphagnum* can also

* Corresponding author at: Organic Geochemistry Unit, School of Chemistry, University of Bristol, Cantock's Close, Bristol BS8 1TS, UK. Tel.: +44 117 9546395.
E-mail address: gordon.inglis@bristol.ac.uk (G.N. Inglis).

http://dx.doi.org/10.1016/j.palaeo.2015.08.001

limit CH_4 emissions by consuming CH_4 symbiotically with aerobic methane-oxidising bacteria (Raghoebarsing et al., 2005; Kip et al., 2010).

A variety of organic geochemical proxies can be used to track changes in peat-forming vegetation, specifically the input of *Sphagnum* moss (Nott et al., 2000; Pancost et al., 2002; Xie et al., 2004; Bingham et al., 2010). *Sphagnum* species are typically dominated by mid-chain C_{23} and C_{25} *n*-alkanes (Baas et al., 2000; Nott et al., 2000), whereas terrestrial, peat-forming higher-plants, such as *Ericaceae* or *Carex*, are dominated by long-chain C_{29} and C_{31} *n*-alkanes (Eglinton and Hamilton, 1967). As such, the C_{23}/C_{31} *n*-alkane ratio has been proposed as a tracer for *Sphagnum* input into ancient peat deposits (Nott et al., 2000; Bingham et al., 2010). A number of studies have shown the close correspondence between the C_{23}/C_{31} *n*-alkane ratio and the relative abundance of *Sphagnum* leaves in a variety of modern ombrotrophic bogs (Nott et al., 2000; Pancost et al., 2002, 2003; Xie et al., 2004). While this has been used to reconstruct vegetation and hydrological change during the Holocene (e.g., Nott et al., 2000), it has not been applied to older peat-forming environments.

In order to investigate ecological, hydrological and biogeochemical change within an early Paleogene peat-forming setting, we reconstruct downcore variations in *Sphagnum* moss within a lignite seam using a high-resolution, multi-proxy approach. Samples are derived from Seam 1, a thermally immature lignite from the Schöningen Südfeld mine, northern Germany (~41 °N palaeolatitude). We use the C_{23}/C_{31} *n*-alkane ratio and the abundance of *Sphagnum*-type spores to reconstruct the occurrence of *Sphagnum* moss. Using this, and other palynological and petrological indicators, we elucidate hydrological change within an early Paleogene peat-forming environment. We then use bacterially-derived hopane distributions and compound-specific carbon isotopes to characterise the biogeochemical response associated with these hydrological changes in a warmer climate.

2. Methods

2.1. Site description

Samples were collected from the Schöningen Südfeld mine in northern Germany, NW Europe (Fig. 1) where the sediments were deposited in a low lying coastal setting (Riegel et al., 2012). Samples are derived from a ~2.7 m thick lignite seam (Seam 1) overlain and underlain by brackish to shallow marine, clastic sedimentary deposits (Riegel et al., 2012). Given the thickness of the seam, we focussed our high-resolution study on the lower and upper part of Seam 1. Samples were collected (c. every 5 cm) from the lower (267 to 200 cm) and upper part of Seam 1 (57 to 0 cm) as well as the overlying brackish to shallow marine interbeds (0 to 36 cm above the seam top). Peat accumulation rates in tropical and subtropical climates are 2 mm/year and 0.8 mm/year, respectively (Collinson et al., 2009 and references therein). Assuming a median peat-to-lignite compaction ratio (7:1) (Ryer and Langer, 1980), Seam 1 spans between 9.5 and 23.6 kyr. The full range, taking the material into account (i.e., woody dominated material vs parenchymatous tissues; Collinson et al., 2009) is 2.7 to 101.2 kyr.

The dinocyst zone D 5nb was recognised above Main Seam in the nearby Emmerstedt area by Ahrendt et al. (1995). If the Main seam is coeval at both sites this would indicate that Seam 1 at Schöningen is earliest Eocene. Within Interbed 2, above Seam 1, there is an abundance of the dinocyst *Apectodinium* (Riegel et al., 2012) which may represent the Paleocene-Eocene Thermal Maximum (PETM) as it does at other sites (Crouch et al., 2003; Sluijs et al., 2007; Sluijs and Brinkhuis, 2009). If so then Seam 1 could be latest Paleocene. However, it should be noted that there are other *Apectodinium* acmes in northern mid-latitude settings during the early Paleogene (see discussion in Collinson et al., 2009, p. 45–51). In summary, we conclude that Seam 1 is of latest Paleocene or earliest Eocene age. Palaeogeographically, Schöningen was located between the Harz Mountains and the Flechtingen Rise at the southern shore of the North Sea during this time interval (Riegel et al., 2012; Fig. 1) at a palaeolatitute of ~41 °N (van Hinsbergen et al., 2015).

2.2. Elemental and bulk $\delta^{13}C$ analyses

Total carbon (TC), total nitrogen (TN) and total hydrogen (TH) analyses were performed using a Carlo Erba EA1108 Elemental Analyser. Total sulphur (TS) analysis was performed in a similar method using a Eurovector EA3000 Analyser. Inorganic carbon (IC) analysis was performed using a Modified Coulomat 702 Analyser with a coulometric cell. Total organic carbon (TOC) content was determined by subtracting IC from TC. Bulk $\delta^{13}C$ analysis was undertaken at Royal Holloway following the methods used by Pancost et al. (2007).

2.3. Organic geochemistry

Approximately 1–10 g of sediment was extracted via Soxhlet apparatus for 24 h using dichloromethane (DCM):methanol (MeOH)

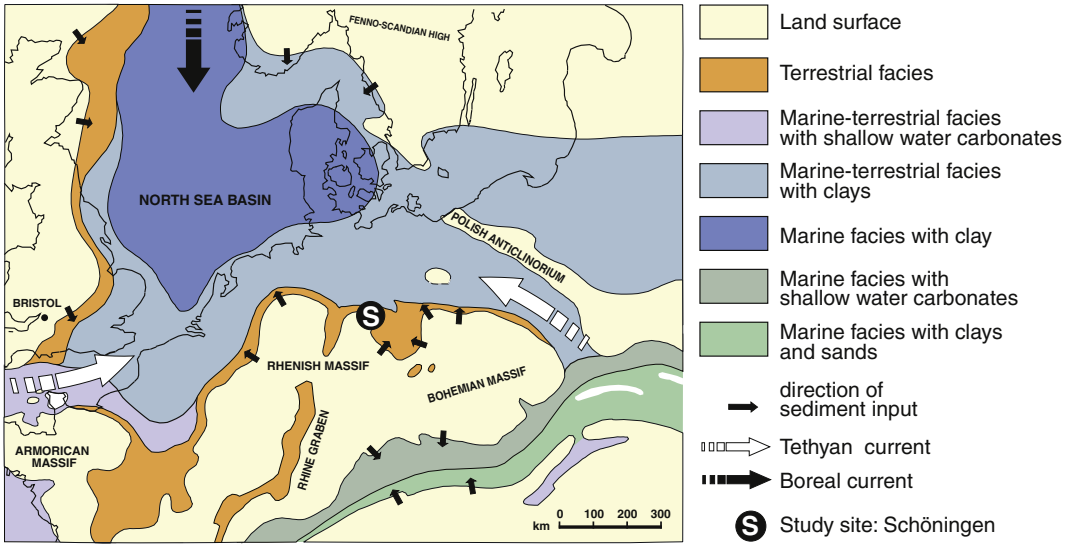

Fig. 1. Palaeogeography of NW Europe during the early Paleogene showing the location of Schöningen. Modified from Riegel et al., 2012.

(2:1 vol/vol) as the organic solvent. The total lipid extract (TLE) was initially separated over silica into neutral and fatty acid fractions using chloroform-saturated ammonia and chloroform:acetic acid (100:1 vol/vol), respectively (Dickson et al., 2009). The neutral fraction was subsequently fractionated over alumina into apolar and polar fractions using hexane:DCM (9:1 vol/vol) and DCM:MeOH (1:2 vol/vol), respectively. All fractions were analysed via gas chromatography–mass spectrometry (GC–MS) using a Thermoquest Finnigan Trace GC interfaced with a Thermoquest Finnigan Trace MS. The electron ionisation source was set at 70 eV. Scanning occurred between m/z ranges of 50 to 650 Da. The GC was fitted with a fused silica capillary column (50 m × 0.32 mm i.d.) coated with a ZB1 stationary phase (dimethylpolysiloxane equivalent, 0.12 μm film thickness). Compound specific carbon isotope analysis was performed on selected apolar fractions using a Trace GC Ultra gas chromatograph coupled to a Finnigan MAT DeltaplusV mass spectrometer via a Finnigan MAT Conflo IV interface. GC Conditions were as for GC–MS. Each value was measured in duplicate and is reported in standard per mil notation (‰) relative to Vienna PeeDee Belemnite (VPDB).

The average chain length (ACL) is defined for *n*-alkanes using the following equation (Eglinton and Hamilton, 1967);

$$\mathrm{ACL} = \frac{(25(n\mathrm{C}_{25}) + 27(n\mathrm{C}_{27}) + 29(n\mathrm{C}_{29}) + 31(n\mathrm{C}_{31}) + 33(n\mathrm{C}_{33})}{(n\mathrm{C}_{25} + n\mathrm{C}_{27} + n\mathrm{C}_{29} + n\mathrm{C}_{31} + n\mathrm{C}_{33})}$$

while the carbon preference index (CPI) is defined using the following equation (Bray and Evans, 1961);

$$\mathrm{CPI} = 0.5 * \left(\frac{n\mathrm{C}_{25} + n\mathrm{C}_{27} + n\mathrm{C}_{29} + n\mathrm{C}_{31}}{n\mathrm{C}_{26} + n\mathrm{C}_{28} + n\mathrm{C}_{30} + n\mathrm{C}_{32}} + \frac{n\mathrm{C}_{27} + n\mathrm{C}_{29} + n\mathrm{C}_{31} + n\mathrm{C}_{33}}{n\mathrm{C}_{26} + n\mathrm{C}_{28} + n\mathrm{C}_{30} + n\mathrm{C}_{32}}\right).$$

The pAq ratio is defined for *n*-alkanes using the following equation (Ficken et al., 2000);

$$\mathrm{pAq} = \frac{n\mathrm{C}_{23} + n\mathrm{C}_{25}}{n\mathrm{C}_{23} + n\mathrm{C}_{25} + n\mathrm{C}_{29} + n\mathrm{C}_{31}}.$$

2.4. Palynology

Approximately 1–2 g of lignite was boiled with 15% hydrogen peroxide (H_2O_2) followed by treatment with 2% potassium hydroxide (KOH). Samples from unconsolidated clastic interbeds were briefly boiled with 15% H_2O_2 and ultrasonicated to separate the organic and mineral matter. In some instances, 2% KOH was added to organic-matter rich clastic samples. Cold hydrofluoric acid was applied for several days in order to remove silica and silicate material from each sample. Samples were then sieved through a 10 μm mesh screen, retaining the coarser fraction. A sub-sample was mounted in glycerine jelly to produce slides subsequently studied by light microscopy. The identification of pollen and spore taxa is based upon previous work (Hammer-Schiemann, 1998). Slides and residues will finally be stored in the palaeobotanical collections of the Senckenberg Forschungsinstitut und Naturmuseum, Frankfurt am Main, Germany.

2.5. Petrology

Petrological study was undertaken only on the lignites of Seam 1 (not on the overlying or underlying siliclastic interbeds). Polished blocks of crushed lignite were prepared to industry standard by Jim Hower and colleagues at the Centre for Applied Energy Research, University of Kentucky using approximately 1–5 g of lignite. Where possible samples were crushed to the standard 20 mesh size, ≤840 μm, using a grinder. Soft samples were crushed manually to a top particle size of c. 1000 μm. A subsample was embedded in epoxy resin. Once dry, the block was polished using 60-, 240-, 400-, and 600-grit SiC papers followed by 0.3-micron alumina on Buehler Texmet paper and 0.05-micron alumina on silk. The finished polished blocks were viewed in reflected light under immersion oil (Cargille type A, density 0.923 g/cc at 23 °C, RI of 1.514) using a Leica reflected light microscope and a ×20 oil immersion objective. Lignite components (maceral groups), huminite, liptinite and inertinite, were classified according to the International Committee for Coal and Organic Petrology (ICCP) standard. Inertinite, recognised by its high reflectance and cellular preservation (ICCP, 2001), is a product of wildfire (Scott, 2002). Huminite, characterised by low reflectance and varied cellular preservation (Sýkorová et al., 2005) indicates how wet or dry the conditions of peat formation were. The huminite maceral ulminite is defined by highly gelified plant material (with homogenous plant cell walls, no visible internal structures and obscured cell lumina) that indicates formation under wet conditions (Sýkorová et al., 2005). Non-gelified huminite macerals attrinite (cemented detrital material) and textinite (cell walls not gelified, open or open but infilled cell lumina) indicate drier conditions during peat formation (Sýkorová et al., 2005). Macerals were quantified following the method outlined in Robson et al. (2015).

3. Results

3.1. Elemental analysis

Total organic carbon (TOC) content within Seam 1 is generally high (>50–60 wt.%; Fig. 2a) with a gradual decrease in the bioturbated upper ~15 cm (15–40 wt.%). TOC values in the overlying marine interbeds are relatively low (3–9 wt.%). C/N ratios are high throughout Seam 1 (50–95; Fig. 2b) with lower values in the overlying marine interbeds (21–37). This is consistent with a terrestrial organic matter source throughout (Boutton, 1991). Total sulphur (TS) content is high throughout Seam 1 (3.9–7.6 wt.%) with lowest values in the overlying marine interbeds (2.1–4.1 wt.%; Fig. 2c). High sulphur contents (e.g., >3 wt.% S) in peat horizons are generally attributed to the incorporation of seawater sulphate into the peat-forming environment (Chou, 2012).

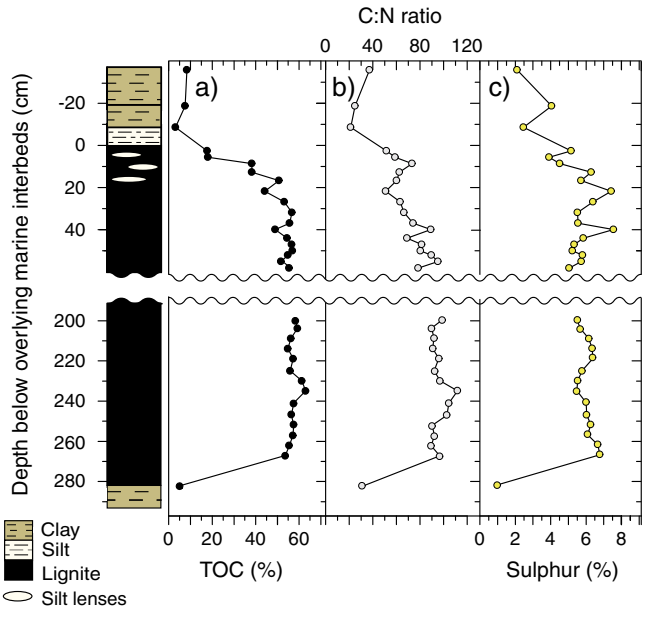

Fig. 2. a) Total organic carbon (%), b) carbon-to-nitrogen (C:N) ratio and c) total sulphur (%) within Seam 1, Schöningen. Zero depth marks the top of Seam 1 and the base of the overlying interbed 2.

3.2. Bulk $\delta^{13}C_{org}$

Bulk $\delta^{13}C_{org}$ values (Fig. 9a, diamonds) were determined for the top of Seam 1 (57–0 cm) and the overlying marine interbeds (0–36 cm). Within the lignite, values range from −25.9‰ to −27.9‰. Within the marine interbeds, values range from −26.5‰ to −27.0‰. Between 57 and 0 cm in Seam 1, bulk $\delta^{13}C_{org}$ values exhibit a gradual upwards decrease in $\delta^{13}C$ by ~1‰.

3.3. Plant-derived biomarkers

Plant biomarkers, including a range of *n*-alkyl and terpenoid components, dominate all of the lipid fractions analysed. The apolar fraction is characterised by a homologous series of *n*-alkanes with a strong odd-over-even predominance (Figs. 3, 4a). Long-chain (C_{27}–C_{31}) homologues, typically derived from the epicuticular wax of higher plants, are the most abundant (2 to 65 μg/g dry sediment). A terrestrial plant origin is confirmed by the *n*-alkane carbon preference index (CPI), which on average is 5.9 (Bray and Evans, 1961; Eglinton and Hamilton, 1967). The average *n*-alkane chain length (ACL) ranges from 26.8 to 29.8 within Seam 1 and is typical for modern tree species (Diefendorf et al., 2011). Mid-chain homologues (C_{23}–C_{25}), derived from submerged and floating macrophytes (Ficken et al., 2000) and/or *Sphagnum* moss (Baas et al., 2000; Nott et al., 2000), are also relatively abundant (1 to 32 μg/g dry sediment; Figs. 3–4). The C_{23}/C_{31} *n*-alkane ratio (Fig. 7a), which is commonly used to trace the input of *Sphagnum* moss to Holocene peat (e.g., Nott et al., 2000), ranges from 0.1 to 6.6 within Seam 1. Short-chain (C_{17}–C_{21}) homologues, typically derived from marine algae, are of low abundance throughout (<1 to 14 μg/g dry sediment; Figs. 3–4).

The apolar fraction also contains a variety of di- and triterpenoids. Diterpanes of the abietane and pimarane class are abundant within Seam 1 between 57 and 43 cm, especially fichtelite, norisopimarane and retene. These compounds are non-specific conifer biomarkers (Otto and Simoneit, 2001). Tetracyclic triterpanes, which are derived from angiosperms and/or gymnosperms (Diefendorf et al., 2014), were identified but are in low abundance. Pentacyclic triterpenoids derived from angiosperms (Simoneit et al., 1986; Otto et al., 2005) are abundant throughout, especially ring-A monoaromatic triterpenoids (Jacob et al., 2007; Fig. 3).

The polar fraction contains mid- and long-chain *n*-alkanols (C_{20}–C_{32}) with a strong even-over-odd predominance (Fig. 4b). The average chain length ranges from 24.7 to 27.1 and the dominant *n*-alkanol is C_{26} or C_{28}. This is consistent with a mixed contribution from *Sphagnum* moss and peat-forming plants such as *Ericaceae* (Ficken et al., 2000; Pancost et al., 2002). This presence of peat-forming plants other than *Sphagnum* is consistent with the identification of amyrenone, a triterpenoid ketone frequently found in angiosperms. An unknown compound with M + 438 and m/z 203 was identified and is also likely derived from angiosperms (Stefanova et al., 2008). The fatty acid fraction contains mid- and long-chain *n*-alkanoic acids (C_{24}–C_{32}) with a strong even-over-odd predominance (Fig. 4c). The average chain length ranges from 25.6 to 28.0 and the dominant *n*-alkanoic acid is C_{28}. This is consistent with terrestrial plant source (Eglinton and Hamilton, 1967). The fatty acid fraction contains trace quantities of short-chain *n*-alkanoic acids (C_{16}–C_{18}) which can have a bacterial or plant-derived source (Baas et al., 2000).

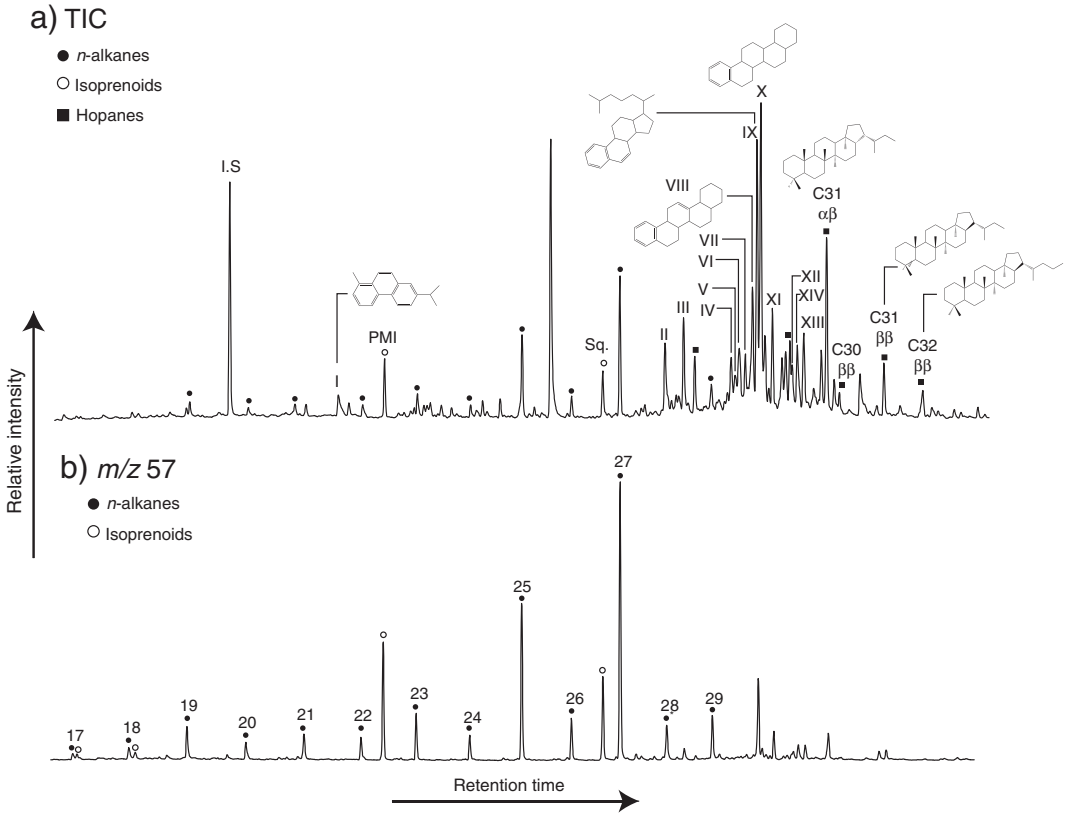

Fig. 3. Partial gas chromatogram of a typical, lignite-derived apolar fraction. a) TIC. Roman numerals denote plant-derived diterpenane and triterpene derivatives (Jacob et al., 2007). I: Retene, II and III: Unknown Ring-A monoaromatic triterpenoid, IV: Dinor-oleana(ursa)-1,3,5(10),13(18)-tetraene, V, VI and VII: Unknown Ring-A monoaromatic triterpenoid, VIII Dinor-oleana(ursa)-1,3,5(10),12-tetraene, IX: Lanosta(eupha)pentaene, X: Dinor-oleana(ursa)-1,3,5(10)-triene, XI: Dinor-oleana(ursa)-1,3,5(10),13(18)-tetraene, XII: Tetranor-oleana(ursa)-1,3,5(10),6,8,11,13-heptaene, XIII: Tetranor-oleana(ursa)-1,3,5(10),6,8,11,13-heptaene, XIV: Tetranor-lupa-1,3,5(10),6,8,11,13-heptaene. Numbers accompanied with Greek letters signify the carbon number and the C-17 and C-21 stereochemistry of bacterial hopanes. b) *m/z* 57 trace showing isoprenoids (open circles) and *n*-alkanes (closed circles).

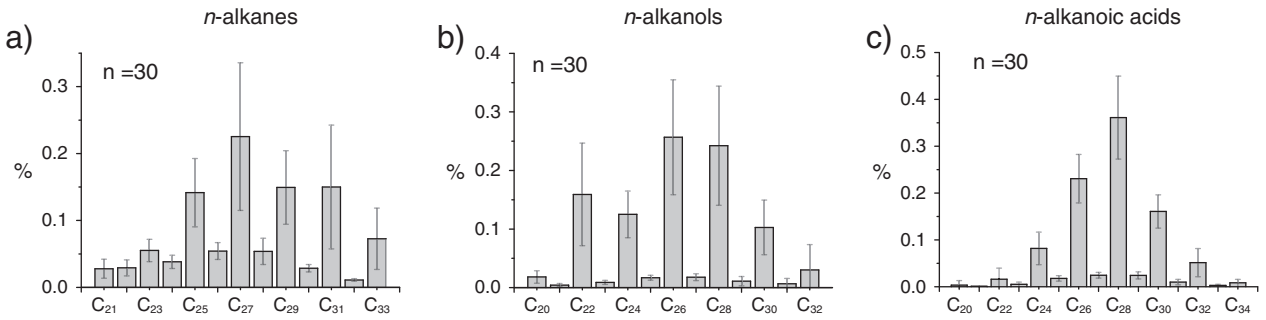

Fig. 4. The average fractional abundance of a) *n*-alkanes, b) *n*-alkanols and c) *n*-alkanoic acids within Seam 1 (n = 30). Error bars reflect one standard deviation.

Compound specific carbon isotope ($\delta^{13}C$) analysis was performed upon a selection of apolar, plant-derived biomarkers from the top of Seam 1 and the overlying marine interbeds (n = 18). In some samples, co-elution of other compounds prevents the determination of $\delta^{13}C$ values. The $\delta^{13}C$ value of long-chain (C_{27}–C_{29}) *n*-alkanes within Seam 1 (Figs. 5 and 9a) ranges from −29.4 to −32.5‰, consistent with a C_3 higher-plant origin (Collister et al., 1994) and values typically observed in ombrotrophic bogs (Pancost et al., 2000). The $\delta^{13}C$ value of mid-chain (C_{23}–C_{25}) *n*-alkanes (Figs. 5 and 9a) is slightly heavier, ranging from −27.9 to −30.5‰ and is consistent with a contribution from a partially submerged source (Ficken et al., 2000). The $\delta^{13}C$ values are summarised in Fig. 5.

3.4. Bacterial-derived biomarkers

The apolar fraction contains abundant C_{27}–C_{32} hopanes (Fig. 3). C_{33}–C_{35} hopanes were also identified but were a relatively minor constituent. Both are derived from the cell membrane of prokaryotes (Ourisson and Albrecht, 1992; Sinninghe Damsté et al., 1995). Total hopane ββ/(ββ + αβ + βα) ratios are relatively high (0.46–0.81), indicating that the samples are relatively immature. C_{31} homohopane ββ/(ββ + αβ + βα) ratios exhibit the same temporal trends as the total hopanes but are significantly lower (0.15–0.53). This does not reflect thermal maturity but rather the production of high amounts of C_{31} αβ homohopane, the dominant hopane in recent (<10 ka), thermally immature, ombrotrophic peat bogs (Quirk et al., 1984; Dehmer, 1993, 1995; Pancost and Sinninghe Damsté, 2003).

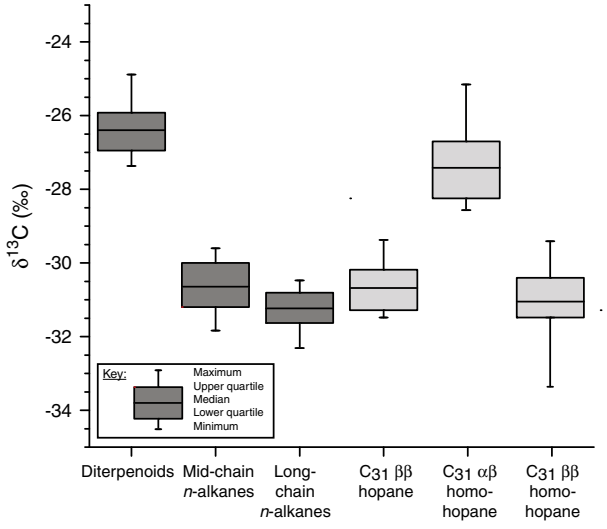

Fig. 5. $\delta^{13}C$ value of plant-derived (dark grey) and microbial-derived (light grey) biomarkers within the top of Seam 1 (0–54 cm) and the overlying marine interbeds (0–36 cm).

Compound specific carbon isotope ($\delta^{13}C$) analysis was performed on a selection of apolar, bacterial-derived biomarkers from the top of Seam 1 (n = 18). In some samples, co-elution of other compounds prevents the determination of $\delta^{13}C$ values. The $\delta^{13}C$ values of the C_{31} ββ homohopane range from −29.1 to −33.1‰. Values of the C_{30} ββ hopane are similar, ranging from −29.1 to −31.2‰. The C_{31} αβ homohopane is ^{13}C-enriched relative to both the C_{31} ββ homohopane and the C_{30} ββ hopane and ranges from −24.9 to −30.4‰. The $\delta^{13}C$ values are summarised in Fig. 5.

3.5. Palynology

Within Seam 1, the dominant plant types represented by palynomorphs are *Sphagnum* moss as indicated by the abundance of *Sphagnum*-type spores (Fig. 6) (especially *Tripunctisporis*, originally used as a subgenus of the widely used but invalid genus *Stereisporites*), ferns (e.g., *Laevigatosporites* — Fig. 7b), swamp-dwelling conifers (e.g., *Inaperturopollenites* — Fig. 7a) and mixed mesopytic forest vegetation (e.g., *Tricolporopollenites cingulum*). Seam 1 is traceable over a few kilometres and the relative abundance of *Sphagnum*-type spores exhibits a similar change in relative abundance through the seam in all three sections studied (Hammer-Schiemann, 1998). In this section, consistently low values occur in the lower part of the seam between 200 and 267 cm (0–10%) with a large increase in abundance in the upper part between 0 and 57 cm (7–48%) (Fig. 7b). During the latter interval, *Sphagnum*-type spores comprise, on average, ~21% of the entire palynological assemblage. *Sphagnum*-type spores are absent or in very low abundance within the overlying marine interbeds (<0.3%). Ferns, specifically *Laevigatosporites* (Fig. 8b) are abundant between 57 and 43 cm (~10.6%) while *Inaperturopollenites* (Fig. 8a) proliferates within the overlying interbeds (~32%).

The dinoflagellate cyst *Apectodinium* (Fig. 8f) tentatively identified as *A. homomorphum* (Riegel et al., 2012), is abundant just above the base of marine interbed 2 where it comprises 13–45% of the entire palynomorph assemblage. Within Seam 1, small quantities of *Apectodinium* occur between 12 and 2 cm (<2%), likely as a result of bioturbation penetrating down into the seam from the overlying interbed. Resting cysts of the freshwater green-algal family Zygnemataceae (Fig. 8f) are present between 21 and 2 cm (<2%), but absent within the overlying marine interbeds and the rest of Seam 1.

3.6. Petrology

Lignite is composed of macerals that are microscopically recognisable fragments of organic matter. Of the three main maceral groups, huminite was the most abundant group within Seam 1 (69.3%), ranging from 53 to 87%. Liptinite was the second most abundant (20.9%), ranging from 9.9 to 30.8% while inertinite (Fig. 8d) was the least abundant (9.8%), ranging from 0.8 to 23.8%. Within the huminite maceral group, three macerals were quantified; attrinite, textinite and ulminite. Attrinite was the most abundant (33.7%), ranging from 15.4 to 48.8%. Textinite was the second most abundant (27.1%), ranging from 12.5 to 60.7% while ulminite

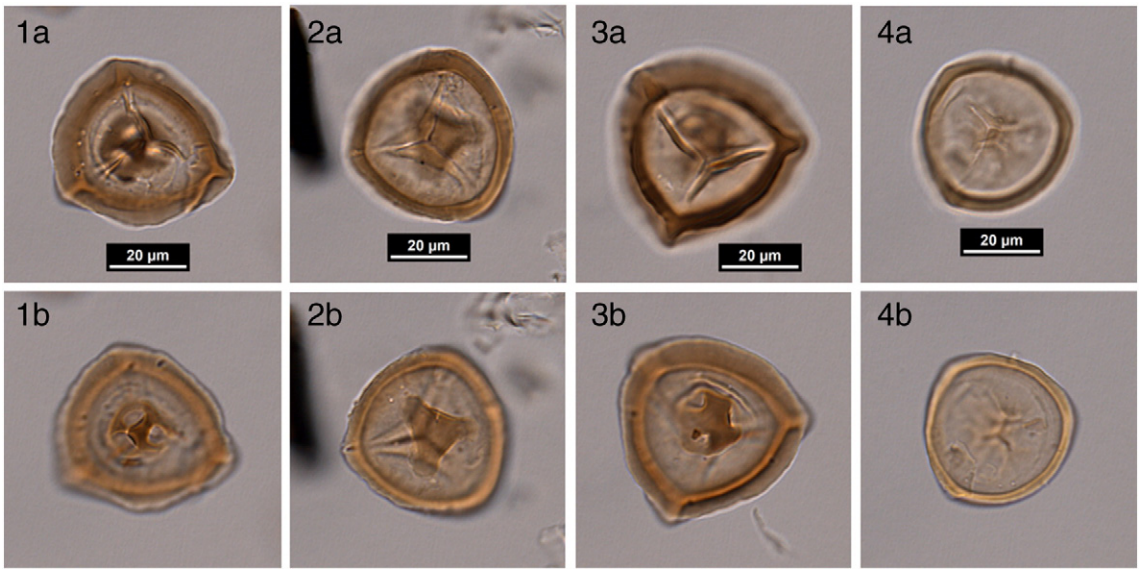

Fig. 6. *Sphagnum*-type spores from Seam 1. 1) *Tripunctisporis* sp. (a—proximal, b—distal), 2) *Distancoraesporis* sp. (a—proximal, b—distal), 3) Transitional form between *Tripunctisporis* and *Distancoraesporis* (a—proximal, b—distal), 4) *Sphagnumsporites* sp. (a—proximal, b—distal).

(Fig. 7c) was the least abundant (8.3%), ranging from 0.8 to 21.4%. On a macroscopic scale, lignites in both the upper and lower parts of Seam 1 are composed of a mix of matrix and tissue lithotypes, but recognisable plant tissue (uncharred) is more common in the lower part of the sequence and charcoal is more common in the upper part. Lithotypes in which charcoal was visible in the field contain higher inertinite percentages in the related polished block containing a crushed sample, in comparison to samples in which no field charcoal was visible.

4. Discussion

4.1. Evidence for the occurrence of Sphagnum in Seam 1, Schöningen

The C_{23}/C_{31} *n*-alkane ratio is used as a chemotaxonomic proxy for *Sphagnum* input in modern peat-forming environments (Baas et al., 2000; Nott et al., 2000; Pancost et al., 2002; Bingham et al., 2010) and is often supplemented with other proxies (e.g., pollen or leaf assemblages)

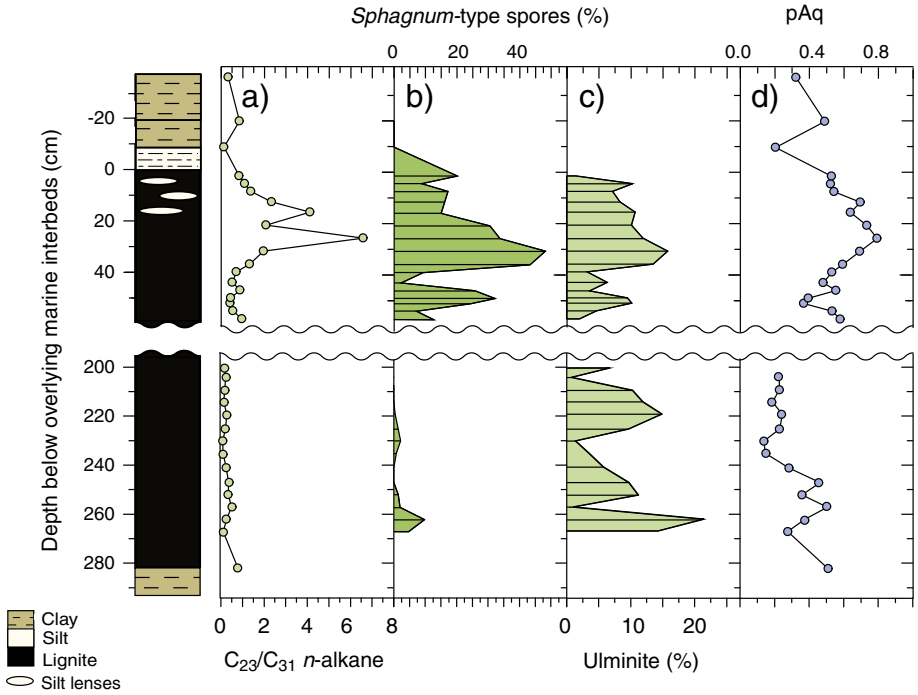

Fig. 7. *Sphagnum* moss occurrence and hydrological change within Seam 1, Schöningen. a) C_{23}/C_{31} *n*-alkane ratio, b) the relative abundance (total palynomorphs) of *Sphagnum*-type spores, c) the relative abundance of ulminite and d) the pAq ratio (the relative abundance of mid-chain *n*-alkanes). Zero depth marks the top of Seam 1 and the base of the overlying interbed 2. Petrology data (ulminite) has only been obtained for lignite.

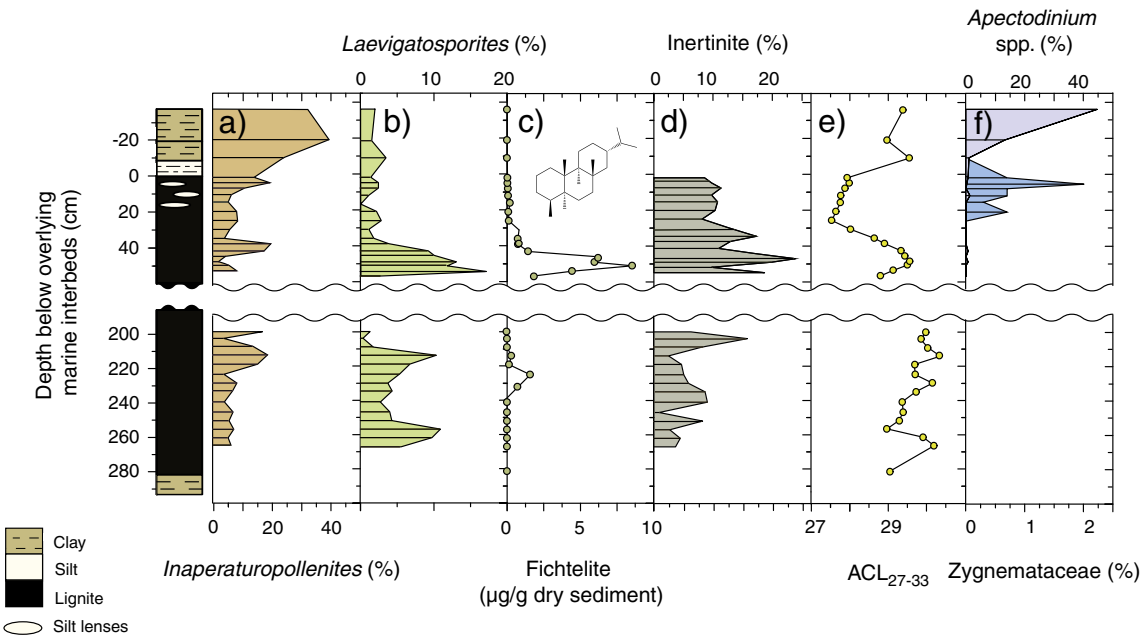

Fig. 8. Key plant groups, hydrology and sea level inundation within Seam 1, Schöningen. The relative abundance (total palynomorphs) of a) *Inaperaturopollenites* (swamp conifer pollen) and b) *Laevigatosporites* (fern spores), c) Fichtelite (conifer biomarker), d) Inertinite (fossil charcoal), e) C_{27}–C_{33} *n*-alkane average chain length (ACL) and f) the relative abundance (total palynomorphs) of the dinoflagellate *Apectodinium* (grey) and freshwater green algal cysts of the family Zygnemataceae (blue). Zero depth marks the top of Seam 1 and the base of the overlying interbed 2. Petrology data (inertinite) has only been obtained for lignite.

to reconstruct vegetation change during the Holocene (e.g., Nott et al., 2000). Here we compare biomarker and palynological downcore trends in order to investigate the distribution and occurrence of *Sphagnum* moss within an early Paleogene, peat-forming environment.

Spores assigned to *Sphagnum* moss are present in most seams of the early Eocene Schöningen Formation (Riegel et al., 2012). They are most commonly represented by *Tripunctisporis*, a former subgenus of the invalid genus *Stereisporites*; however, at least three to four morphotaxa of *Sphagnum*-type spores can be distinguished (i.e., *Tripunctisporis* and *Distancoraesporis* plus a number of forms more closely resembling modern *Sphagnum* spores; Fig. 6). *Tripunctisporis* differs slightly from spores of modern *Sphagnum*, but its co-occurrence with charred remains of *Sphagnum*-leaves in a thin lignite seam within interbed 4 (Riegel et al., 2012) confirms a likely *Sphagnum* origin as originally suggested by Döring et al. (1966). The proportion in which *Sphagnum*-type spores contribute to the frequency curve (Fig. 7) varies without any obvious pattern to it. However, *Tripunctisporis* and *Distancoraesporis* dominate in most of the samples. *Sphagnum*-type spores are low or absent within the base of Seam 1 (200–267 cm; <10%). This is consistent with low C_{23}/C_{31} *n*-alkane values (~0.4) which indicate that *Sphagnum* moss was probably not an important component of the peat-forming vegetation within this interval (Fig. 7). The pAq ratio (Fig. 7d), which can also be used to infer changes in *Sphagnum* occurrence and local hydrology (Nichols et al., 2006), averages 0.27 and ranges from 0.13 to 0.50 within the base of Seam 1 (200–267 cm). This suggests mixed input from terrestrial higher plants, dominated by C_{29} and C_{31} *n*-alkanes, and *Sphagnum* moss, dominated by C_{23} and C_{25} *n*-alkanes. Submerged and/or floating freshwater aquatic macrophytes can also produce mid-chain *n*-alkanes and may contribute towards the observed pAq values (Ficken et al., 2000).

Within the top of Seam 1 (0–57 cm), *Sphagnum*-type spores increase significantly and comprise 20 to 50% of the entire palynological assemblage. During the same interval, the C_{23}/C_{31} *n*-alkane ratio increases (~1.6) and yields values that are typical of a modern, *Sphagnum*-dominated bog (Nott et al., 2000; Pancost et al., 2002; Xie et al., 2004; Bingham et al., 2010). The similarity between biomarkers and palynology (Fig. 7) provides compelling evidence that *Sphagnum* moss was an important peat-forming plant within the top of Seam 1 (0–57 cm) and that the C_{23}/C_{31} *n*-alkane ratio is a reliable chemotaxonomic indicator for *Sphagnum* input during the early Paleogene. *Sphagnum* expansion coincides with an increase in the pAq ratio (0.52 to 0.79; Fig. 7d) and a decrease in the *n*-alkane average chain length (ACL; Fig. 8e). The latter is consistent with modern studies which exhibit a similar decrease during the transition from *Ericaceae* to *Sphagnum*-dominated peat (Pancost et al., 2003).

Sphagnum-type spores are typically absent (Collinson et al., 2009) or rare (Wilson and Webster, 1946; Nichols and Traverse, 1971; Jardine and Harrington, 2008) within early Paleogene peat-forming environments. However, the similarity between *Sphagnum* biomarkers and *Sphagnum*-type spores within Seam 1, suggests a deeper evolutionary origin for *Sphagnum* moss. This is supported by the identification of *Sphagnum* leaves and/or spores in other Cenozoic (Jie and Xiuyi, 1986) and Mesozoic (Lacey, 1969) terrestrial settings.

4.2. Environmental controls on Sphagnum occurrence within Seam 1, Schöningen

In modern settings, *Sphagnum* is adapted to acidic, waterlogged and nutrient-limited environments and its occurrence is largely controlled by changes in local hydrology (van Breemen, 1995). To assess the role of hydrological change upon ancient *Sphagnum* occurrence, we use biomarkers, palynology and petrological evidence to constrain hydrological and environmental change within Seam 1.

While the low abundance of *Sphagnum*-type spores and biomarkers within the base of Seam 1 (200–267 cm; Fig. 7) suggests relatively dry conditions (Clymo, 1984), lignite macerals can provide further insights into local hydrological change. Attrinite, which forms in relatively dry conditions at the mire surface (Sýkorová et al., 2005), is the most abundant maceral within the base of Seam 1 (~34%) and suggests relatively dry conditions. Textinite, which also forms in relatively dry, possibly low pH environments within forested peatlands and/or raised bogs (Sýkorová et al., 2005), is similarly abundant within the base of Seam 1 (~27%) and indicates a relatively dry environment.

Within the top of Seam 1, between 57 and 46 cm, there is a transient increase in conifer biomarkers (e.g., fichtelite: Fig. 8c) and fern spores (e.g., *Laevigatosporites* spp.; Fig. 8b), likely indicating the expansion of conifer forests with a fern understory. This is associated with an increase in the relative abundance of inertinite (i.e., fossil charcoal), suggesting increased wildfire activity. Between 46 and 20 cm, there is an increase in the relative abundance of *Sphagnum*-type spores (>20%) and C_{23}/C_{31} *n*-alkane ratios (>1) (Fig. 7a, b) indicating the development of waterlogged, nutrient-limited conditions. This is consistent with other early Paleogene, peat-forming environments where *Sphagnum*-type spores proliferate following changes in basin subsidence and drainage (Pocknall, 1987). Ulminite, which forms in wet, low pH conditions within forested peatlands or raised bogs (Sýkorová et al., 2005), correlates with the relative abundance of *Sphagnum*-type spores throughout the top of Seam 1 (Fig. 7b,c) and provides additional evidence that *Sphagnum* occurrence was driven by the expansion of waterlogged conditions. Although some *Sphagnum* taxa can thrive in more mesotrophic, low-lying swamps (e.g., *Sphagnum russowii* or *Sphagnum riparium*), the abundance of ulminite and the distribution of bacterial hopanoids is more consistent with an acidic, oligotrophic peat-forming environment (see later). Inertinite relative abundance remains high throughout this upper part of the seam (Fig. 8d). This suggests that fire activity may have played a role in maintaining *Sphagnum* relative abundance by impeding the spread of taller, hence more vulnerable, vascular plants across the bog surface.

The relative abundance of *Sphagnum*-type spores (<30%) and the C_{23}/C_{31} *n*-alkane ratio (<2) decreases within the very top of Seam 1 (20–0 cm). This interval coincides with a decrease in the *n*-alkane ACL and the incursion of green algae (Zygnemataceae — Fig. 8f) associated with standing freshwater environments. This suggests that freshwater flooding restricted the growth of higher plants and, to a lesser extent, mosses. Peat-deposition is eventually terminated by a brackish, shallow-water incursion as indicated by the presence of *Apectodinium* — Fig. 8f, a marine dinoflagellate cyst associated with shallow subtropical waters, within interbed 2. Sea level inundation was either driven by changes in local basin subsidence (i.e., an increase in accommodation space) associated with regional passive salt withdrawal towards the Helmstedt-Stassfurt Salt Wall during the early and middle Eocene (Brandes et al., 2012), changes in terrestrial run-off associated with a warmer climate (Slotnick et al., 2012) and/or eustatic sea level rise (Riegel et al., 2012).

4.3. Insights into the biogeochemistry of Paleogene ombrotrophic bogs

Modern ombrotrophic bogs are characterised by a distinct microbial assemblage that is associated with the unusual dominance of the C_{31} 17α,21β(H) homohopane (Quirk et al., 1984; Dehmer, 1993, 1995; Pancost and Sinninghe Damsté, 2003). This isomer is common in high maturity sediments (Seifert and Moldowan, 1980) and, with the exception of the soil bacterium *Frankia* spp. (Rosa-Putra et al., 2001), is not synthesised by living organisms. Its occurrence within modern peat deposits has therefore been attributed to rapid isomeric catalysation at the C-17 position as a result of acidic conditions (van Dorselaer et al., 1975; Dehmer, 1993, 1995; Pancost et al., 2003), although a biological origin remains possible. The ratio of the C_{31} 17β,21β(H) homohopane to total homohopanes (=ββ/αβ + ββ) in modern peats ranges from <0.01 to 0.85 and averages ~0.1 (Pancost et al., 2003; Inglis, G. unpublished). Within Seam 1, Schöningen, the C_{31} 17α,21β(H) homohopane is the dominant hopane (Fig. 3) and the ββ/αβ + ββ ratio ranges from to 0.16 to 0.57, averaging 0.27. The C_{31} 17α,21β(H) homohopane is also a major constituent of other thermally immature Cenozoic lignites (Dehmer, 1988; Pancost et al., 2007). This suggests that diagenetic reactions and/or bacterial communities within Seam 1 and other ancient peat-forming environments are similar to those of Holocene wetlands. By extension, in relatively immature, marginal marine sediments, low ββ/αβ + ββ ratios could also serve as a useful new proxy for the input of peat (or eroded lignite).

The $\delta^{13}C$ values of bacterial hopanoids can also provide insights into microbial methane cycling. The carbon isotopic composition ($\delta^{13}C$) of the C_{31} 17α,21β(H) homohopane in modern *Sphagnum*-dominated bogs is typically enriched in ^{13}C (−22 to −26‰) relative to bulk organic matter and plant-derived *n*-alkanes (Pancost et al., 2000; Inglis, G. unpublished). This likely indicates a heterotrophic bacterial population consuming ^{13}C-enriched carbohydrates (Pancost et al., 2000; Xie et al., 2004). In the same setting, the $\delta^{13}C$ value of C_{32} 17β,21β(H) bishomohopanol is lower, ranging from −27‰ to −30‰, perhaps suggesting a mixed suite of bacterial sources consuming both ^{13}C-enriched carbohydrates and ^{13}C-depleted, methane-derived CO_2 (Pancost et al., 2000). In some cases, however, the $\delta^{13}C$ value of extended hopanoids can be depleted in ^{13}C; in particular, van Winden et al. (2010) reported $\delta^{13}C$ values of C_{32} ββ bishomohopanol in extant *Sphagnum* species ranging from −34‰ to −37‰, suggesting that they partially derive from symbiotic methanotrophs. The lowest modern $\delta^{13}C$ values are derived from diploptene (C_{30} 17β, 21β (H)-hop-22(29)-ene) within a *Carex*-dominated bog where $\delta^{13}C$ values range between 31.6‰ and −50.3‰ (Zheng et al., 2014).

In another Paleogene wetland deposit, the Cobham Lignite (~56 Myr ago), the $\delta^{13}C$ values of the C_{29}- and C_{31}-17β(H),21β(H) hopane decrease dramatically (to values as low as −76‰ and −42‰, respectively) in response to freshwater flooding and indicates the consumption of isotopically light methane by aerobic methanotrophs (Pancost et al., 2007). Such values have yet to be observed in a modern or Holocene peat deposit, but they are consistent with modelled wetland methane emissions, which suggest a ~6- to 7-fold increase during Paleogene warm climates (Beerling et al., 2011). To investigate this further, we generate hopane $\delta^{13}C$ values within the top of Seam 1 and use this to reconstruct the relative amount of aerobic methanotrophy within an early Paleogene, peat-forming environment.

Within the top of Seam 1 the $\delta^{13}C$ value of the C_{31} 17α,21β(H) hopane ranges between −24.9‰ and −28.3‰ (Fig. 9b). These values are similar

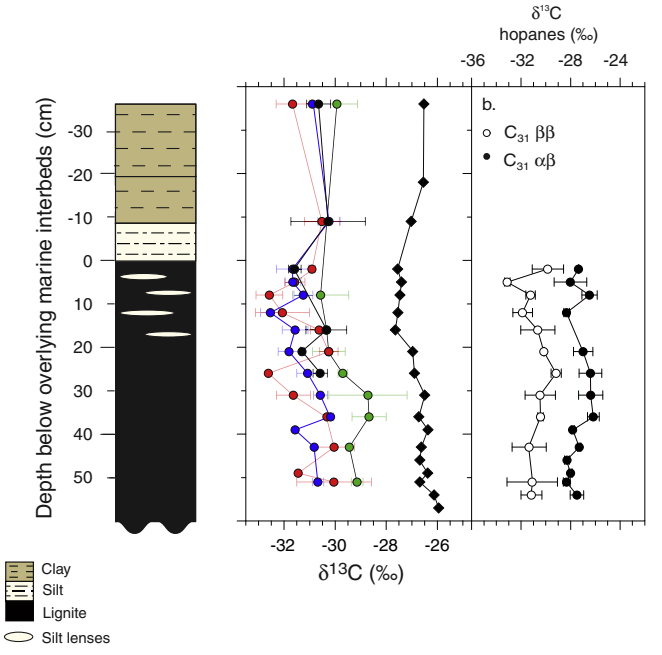

Fig. 9. Isotopic change within the top of Seam 1 (0–57 cm) and the overlying marine interbeds (0–36 cm). a) Bulk $\delta^{13}C_{V\text{-}PDB}$ values (C_{org}; black diamonds) and compound-specific isotope $\delta^{13}C_{V\text{-}PDB}$ values for mid- and long-chain *n*-alkanes (C_{23}; green circles, C_{25}; red circles, C_{27}; blue circles, C_{29}; black circles). b) Compound-specific isotope $\delta^{13}C_{V\text{-}PDB}$ values for bacterial-derived hopanes. Zero depth marks the top of Seam 1 and the base of the overlying interbed 2.

to those observed in modern ombrotrophic bogs (−22‰ to −26‰; Pancost et al., 2000) and suggest a similar source organism and ecology. The $\delta^{13}C$ value of the C_{30}- and C_{31}-17β,21β(H) hopane ranges between −28 and −32‰ (Figs. 5 and 9b). These values are persistently 2–10‰ lighter than modern C_{31} 17α,21β(H) hopane $\delta^{13}C$ values and are more consistent with modern C_{32} ββ bishomohopanol $\delta^{13}C$ values (−27‰ to −30‰; Pancost et al., 2000). This suggests that the C_{30}- and C_{31}-17β,21β(H) hopanes are derived from a mixed methanotrophic and heterotrophic bacterial population (van Winden et al., 2012). Such relatively low values persist through the top 54 cm of Seam 1 – likely reflecting 1.8 to 4.7 kyr – and could indicate a somewhat more intense methane cycling regime than observed in boreal Holocene bogs (cf. Pancost et al., 2000). However, unlike the Cobham Lignite (Pancost et al., 2007) or even some Holocene studies (Zheng et al., 2014), very low $\delta^{13}C$ hopane values were not observed suggesting that the top of Seam 1 was not characterised by extensive aerobic methanotrophy. Hopane $\delta^{13}C$ values are relatively invariant throughout the top of Seam 1, despite an increase in *Sphagnum* abundance and waterlogged conditions (see Section 4.1). This could potentially be attributed to the absence of symbiotic methane-oxidising bacteria (Raghoebarsing et al., 2005; Kip et al., 2010). Alternatively, the incursion of sulphate-rich marine waters may suppress the rate of methanogenesis (Whiticar, 1999). This hypothesis is consistent with the presence of *Apectodinium* within the overlying marine interbeds and high elemental sulphur concentrations throughout the seam (3.9–7.6 wt.%; Fig. 2c) (Chou, 2012). Recent work has also shown that low $\delta^{13}C$ hopane values are not necessarily associated with an increase in waterlogged conditions (cf. Van Winden et al., 2012). For example, Zheng et al. (2014) show that low $\delta^{13}C$ hopane values (−42‰ to −50‰) are associated with a pronounced dry interval during the mid-Holocene. This likely reflects changes in methane flux pathways and more efficient methane oxidation under drier conditions (Zheng et al., 2014). By extension, the absence of very low $\delta^{13}C$ hopane values at Schöningen could reflect less efficient methane oxidation under wetter conditions (cf. Zheng et al., 2014).

In modern, ombrotrophic, *Sphagnum*-dominated bogs, the carbon isotopic composition of the C_{23} *n*-alkane can also provide insights into the amount of aerobic methanotrophy. In modern bogs, the C_{23} *n*-alkane can be depleted in ^{13}C (~5–10‰) relative to high molecular weight (C_{29}–C_{33}) *n*-alkanes (Brader et al., 2010; van Winden et al., 2010; Huang et al., 2014), suggesting incorporation of ^{13}C-depleted, CH_4-derived CO_2 associated with aerobic methanotrophy (Kip et al., 2010; van Winden et al., 2010). However, in other ombrotrophic bogs, the C_{23} *n*-alkane does not exhibit ^{13}C-depleted values (−30‰ to −33‰; Pancost et al., 2003). In the same study, mid-chain *n*-alkanols, which can also be derived from *Sphagnum*, did not exhibit ^{13}C-depleted values, ranging from −30‰ to −33‰ (e.g., Pancost et al., 2003). Within the top of Seam 1, the $\delta^{13}C$ value of the C_{23} *n*-alkane ranges from −28.7‰ to −30.6‰. These values are ^{13}C-enriched (1–2‰) relative to HMW *n*-alkanes (−30.1‰ to −32.5‰) and are consistent with a partially submerged source (Ficken et al., 2000; Pancost et al., 2003). This indicates relatively low rates of aerobic methanotrophy within Seam 1 despite overall wetter conditions. Both mid- and long-chain *n*-alkanes exhibit gradual ^{13}C-depletion towards the top of Seam 1, consistent with bulk $\delta^{13}C$ values (Fig. 9a). During the same interval, hopane $\delta^{13}C$ values remain relatively invariant. This suggests that mid- and long-chain *n*-alkane ^{13}C-depletion cannot be attributed to a rise in the water table but instead may be the consequence of some other mechanism (e.g., changes in CO_2, plant growth rate and/or temperature). Collectively, both hopanes and mid-chain *n*-alkanes do not indicate significantly enhanced methanotrophy in this early Paleogene, peat-forming environment, in contrast to the Cobham lignite (Pancost et al., 2007). The reason for this remains unclear but may be related to site-specific differences. For example, the top of Seam 1, Schöningen suggests the presence of intermittent marine conditions. This is based upon high elemental sulphur concentrations (>4% wt.) and the presence of silt and/or sand lenses (Figs. 2c and 7). In contrast, the Cobham lignite sequence was deposited under a freshwater environment as indicated by the absence of dinoflagellate cysts and *Ophiomorpha* burrows and the presence of freshwater wetland flora (Collinson et al., 2009). Despite this, the biogeochemical response associated with flooding ancient peat-forming environments remains poorly constrained and requires further investigation.

These results indicate the complexity of methane cycling within ancient peat-forming environments; however, changes in methane concentrations remain an important positive feedback mechanism during the early Eocene. For example, earth system modelling simulations indicate that early Eocene methane emissions may have been up to 6× greater than the modern. This can account for up to ~6 °C of high-latitude warming (Beerling et al., 2011) and has implications for numerical model studies which often fail to replicate high-latitude, proxy-derived temperature estimates (Huber and Sloan, 2001; Hollis et al., 2012; Lunt et al., 2012). Enhanced methane emissions can also promote the formation of thick, polar stratospheric clouds (Sloan and Pollard, 1998) which may account for enhanced high-latitude warmth during the early Eocene and other greenhouse intervals (Sloan et al., 1992).

5. Conclusion

Using a high-resolution, multi-proxy approach, we reconstruct the occurrence of *Sphagnum* moss within an early Paleogene peat-forming environment (Seam 1, Schöningen Mine, Germany). C_{23}/C_{31} *n*-alkane ratios (<0.4) and the relative abundance of *Sphagnum*-type spores (especially *Tripunctisporis*) are low within the base of Seam 1 (200–267 cm), indicating that *Sphagnum* was not an important peat-forming plant during this interval. Within the top of Seam 1 (57–0 cm), C_{23}/C_{31} n-alkane ratios increase and are comparable to, or exceed, values from modern, *Sphagnum*-dominated ombrotrophic bogs. This coincides with an increase in the relative abundance of *Sphagnum*-type spores which comprise up to 45% of the entire palynological assemblage. Our results show a close association between *Sphagnum* biomarkers and *Sphagnum*-type spores within an early Paleogene peat-forming environment, analogous to what has been observed during the Holocene, and suggest that the C_{23}/C_{31} *n*-alkane ratio may be a reliable chemotaxonomic indicator for *Sphagnum* input during the early Paleogene. Changes in biomarkers, palynology and petrology indicate that *Sphagnum* proliferation was driven by an increase in waterlogged conditions within the top of Seam 1. Increased fire activity may also have played a role by reducing re-colonisation by vascular plants. In comparison to other early Paleogene peat-forming environments, the $\delta^{13}C$ value of bacterial hopanes and plant-derived *n*-alkanes do not indicate significant aerobic methanotrophy. Nor do they indicate a change in methanotrophy despite a rise in the water table. The reason for this difference remains unclear but may be linked to the incursion of sulphate-rich, marine waters which might inhibit methanogenesis and/or reduce the efficiency of methane oxidation.

Acknowledgements

We thank the NERC Life Sciences Mass Spectrometry Facility (Bristol) for analytical support and GNI thanks the NERC for supporting his PhD studentship (NE/I005714/1). RDP acknowledges the Royal Society Wolfson Research Merit Award. We gratefully acknowledge funding to Collinson and Robson from the NERC grant NE/J008656/1 and to Pancost from NERC grant NE/J008591/1. We thank Jim Hower (University of Kentucky) for production of polished blocks of crushed lignite, Karin Schmidt (Senckenberg Forschungsinstitut und Naturmuseum, Frankfurt) for extensive logistical support, especially during field work, Nathalie Grassineau (Earth Sciences, Royal Holloway) for running the bulk carbon isotope samples and David Naafs and Marcus Badger for comments on earlier versions of this manuscript. Finally, we also thank both reviewers

for constructive comments which helped to improve the quality of this manuscript.

References

Ahrendt, H., Köthe, A., Lietzow, A., Marheine, D., Ritzkowski, S., 1995. Lithostratigraphie, Biostratigraphie und radiometrische Datierungen des Unter-Eozäns von Helmstedt (SE-Niedersachsen). Z. Dtsch. Geol. Ges. 146, 450–457.

Baas, M., Pancost, R., van Geel, B., Sinninghe Damsté, J.S., 2000. A comparative study of lipids in *Sphagnum* species. Org. Geochem. 31 (6), 535–541.

Beerling, D.J., Fox, A., Stevenson, D.S., Valdes, P.J., 2011. Enhanced chemistry-climate feedbacks in past greenhouse worlds. Proceedings of the National Academy of Sciences.

Bijl, P.K., Schouten, S., Sluijs, A., Reichart, G.-J., Zachos, J.C., Brinkhuis, H., 2009. Early Palaeogene temperature evolution of the southwest Pacific Ocean. Nature 461 (7265), 776–779.

Bingham, E.M., McClymont, E.L., Väliranta, M., Mauquoy, D., Roberts, Z., Chambers, F.M., Pancost, R.D., Evershed, R.P., 2010. Conservative composition of n-alkane biomarkers in Sphagnum species: implications for palaeoclimate reconstruction in ombrotrophic peat bogs. Org. Geochem. 41 (2), 214–220.

Boutton, T.W., 1991. Stable carbon isotope ratios of natural materials: II. Atmospheric, Terrestrial, Marine, and Freshwater Environments: Carbon Isotope Techniques. vol. 1 p. 173.

Brader, A.V., van Winden, J.F., Bohncke, S.J., Beets, C.J., Reichart, G.-J., de Leeuw, J.W., 2010. Fractionation of hydrogen, oxygen and carbon isotopes in *n*-alkanes and cellulose of three *Sphagnum* species. Org. Geochem. 41 (12), 1277–1284.

Brandes, C., Pollok, L., Schmidt, C., Wilde, V., Winsemann, J., 2012. Basin modelling of a lignite-bearing salt rim syncline: insights into rim syncline evolution and salt diapirism in NW Germany. Basin Res. 24 (6), 699–716.

Bray, E.E., Evans, E.D., 1961. Distribution of n-paraffins as a clue to recognition of source beds. Geochim. Cosmochim. Acta 22 (1), 2–15.

Bridgham, S.D., Cadillo-Quiroz, H., Keller, J.K., Zhuang, Q., 2013. Methane emissions from wetlands: biogeochemical, microbial, and modeling perspectives from local to global scales. Glob. Chang. Biol. 19 (5), 1325–1346.

Chou, C.-L., 2012. Sulfur in coals: a review of geochemistry and origins. Int. J. Coal Geol. 100, 1–13.

Clymo, R., 1984. The limits to peat bog growth. Philos. Trans. R. Soc., B 303 (1117), 605–654.

Collinson, M.E., Steart, D.C., Harrington, G.J., Hooker, J.J., Scott, A.C., Allen, L.O., Glasspool, I.J., Gibbons, S.J., 2009. Palynological evidence of vegetation dynamics in response to palaeoenvironmental change across the onset of the Paleocene–Eocene Thermal Maximum at Cobham, Southern England. Grana 48 (1), 38–66.

Collister, J.W., Rieley, G., Stern, B., Eglinton, G., Fry, B., 1994. Compound-specific $\delta^{13}C$ analyses of leaf lipids from plants with differing carbon dioxide metabolisms. Org. Geochem. 21 (6), 619–627.

Crouch, E.M., Dickens, G.R., Brinkhuis, H., Aubry, M.-P., Hollis, C.J., Rogers, K.M., Visscher, H., 2003. The Apectodinium acme and terrestrial discharge during the Paleocene–Eocene thermal maximum: new palynological, geochemical and calcareous nannoplankton observations at Tawanui, New Zealand. Palaeogeogr. Palaeoclimatol. Palaeoecol. 194 (4), 387–403.

DeConto, R.M., Galeotti, S., Pagani, M., Tracy, D., Schaefer, K., Zhang, T., Pollard, D., Beerling, D.J., 2012. Past extreme warming events linked to massive carbon release from thawing permafrost. Nature 484 (7392), 87–91.

Dehmer, J., 1988. Petrographische und organischgeochemische Untersuchungen an rezenten Torfen und tertiären Braun-kohle—ein Beitrag zur Fazies und Genese gebänderter Braunkohle (Aachen).

Dehmer, J., 1993. Petrology and organic geochemistry of peat samples from a raised bog in Kalimantan (Borneo). Org. Geochem. 20 (3), 349–362.

Dehmer, J., 1995. Petrological and organic geochemical investigation of recent peats with known environments of deposition. Int. J. Coal Geol. 28 (2), 111–138.

Dickson, L., Bull, I.D., Gates, P.J., Evershed, R.P., 2009. A simple modification of a silicic acid lipid fractionation protocol to eliminate free fatty acids from glycolipid and phospholipid fractions. J. Microbiol. Methods 78 (3), 249–254.

Diefendorf, A.F., Freeman, K.H., Wing, S.L., Graham, H.V., 2011. Production of n-alkyl lipids in living plants and implications for the geologic past. Geochim. Cosmochim. Acta 75 (23), 7472–7485.

Diefendorf, A.F., Freeman, K.H., Wing, S.L., 2014. A comparison of terpenoid and leaf fossil vegetation proxies in Paleocene and Eocene Bighorn Basin sediments. Org. Geochem. 71, 30–42.

Döring, H., Krutzsch, W., Schulz, E., Timmermann, E., 1966. Über einige neue Subformgenera der Sporengattung Stereisporites Th. & Pf. aus dem Mesozoikum und dem Tertiär. – Geologie Beiheft. 55 pp. 72–83 Berlin.

Eglinton, G., Hamilton, R.J., 1967. Leaf epicuticular waxes. Science 156 (3780), 1322–1335.

Ficken, K., Li, B., Swain, D., Eglinton, G., 2000. An *n*-alkane proxy for the sedimentary input of submerged/floating freshwater aquatic macrophytes. Org. Geochem. 31 (7), 745–749.

Hammer-Schiemann, G., 1998. Palynologische Untersuchungen zur Fazies und Ökologie der Unterflözgruppe im Tagebau Schöningen (Untereozän, Helmstedt, Bez. Braunschweig.). University of Göttingen (PhD thesis).

Hollis, C.J., Taylor, K.W.R., Handley, L., Pancost, R.D., Huber, M., Creech, J.B., Hines, B.R., Crouch, E.M., Morgans, H.E.G., Crampton, J.S., Gibbs, S., Pearson, P.N., Zachos, J.C., 2012. Early Paleogene temperature history of the Southwest Pacific Ocean: reconciling proxies and models. Earth Planet. Sci. Lett. 349–350, 53–66.

Huang, X., Xue, J., Meyers, P.A., Gong, L., Wang, X., Liu, Q., Qin, Y., Wang, H., 2014. Hydrologic influence on the $\delta^{13}C$ variation in long chain n-alkanes in the Dajiuhu peatland, central China. Org. Geochem. 69, 114–119.

Huber, M., Caballero, R., 2011. The early Eocene equable climate problem revisited. Clim. Past Discuss. 7 (1), 241–304.

Huber, M., Sloan, L.C., 2001. Heat transport, deep waters, and thermal gradients: coupled simulation of an Eocene greenhouse climate. Geophys. Res. Lett. 28 (18), 3481–3484.

ICCP, 2001. The new inertinite classification (ICCP System 1994). Fuel 80 (4), 459–471.

Jacob, J., Disnar, J.R., Boussafir, M., Spadano Albuquerque, A.L., Sifeddine, A., Turcq, B., 2007. Contrasted distributions of triterpene derivatives in the sediments of Lake Caçó reflect paleoenvironmental changes during the last 20,000 yrs in NE Brazil: Organic Geochemistry. v. 38, no. 2, pp. 180–197.

Jardine, P.E., Harrington, G.J., 2008. The Red Hills Mine palynoflora: a diverse swamp assemblage from the late Paleocene of Mississippi, U.S.A. Palynology 32 (1), 183–204.

Jie, L., Xiuyi, Z., 1986. Discovery of Tertiary sphagnum coal in Jinsuo Basin, Yunnan Province and its significance. Kexue Tongbao Sin. 31, 1556–1559.

Kip, N., van Winden, J.F., Pan, Y., Bodrossy, L., Reichart, G.-J., Smolders, A.J.P., Jetten, M.S.M., Damste, J.S.S., Op den Camp, H.J.M., 2010. Global prevalence of methane oxidation by symbiotic bacteria in peat-moss ecosystems. Nat. Geosci. 3 (9), 617–621.

Krishnan, S., Pagani, M., Huber, M., Sluijs, A., 2014. High latitude hydrological changes during the Eocene Thermal Maximum 2. Earth Planet. Sci. Lett. 404, 167–177.

Lacey, W.S., 1969. Fossil bryophytes. Biol. Rev. 44 (2), 189–205.

Lowenstein, T.K., Demicco, R.V., 2006. Elevated Eocene atmospheric CO_2 and its subsequent decline. Science 313 (5795), 1928.

Lunt, D.J., Dunkley Jones, T., Heinemann, M., Huber, M., LeGrande, A., Winguth, A., Loptson, C., Marotzke, J., Roberts, C.D., Tindall, J., Valdes, P., Winguth, C., 2012. A model–data comparison for a multi-model ensemble of early Eocene atmosphere–ocean simulations: EoMIP. Clim. Past 8 (5), 1717–1736.

Nichols, D.J., Traverse, A., 1971. Palynology, petrology, and depositional environments of some early Tertiary lignites in Texas. Proceedings of the Annual Meeting vol. 2. American Association of Stratigraphic Palynologists, pp. 37–48.

Nichols, J.E., Booth, R.K., Jackson, S.T., Pendall, E.G., Huang, Y., 2006. Paleohydrologic reconstruction based on n-alkane distributions in ombrotrophic peat: Organic Geochemistry. v. 37, no. 11, pp. 1505–1513.

Nott, C.J., Xie, S., Avsejs, L.A., Maddy, D., Chambers, F.M., Evershed, R.P., 2000. n-Alkane distributions in ombrotrophic mires as indicators of vegetation change related to climatic variation. Org. Geochem. 31 (2–3), 231–235.

Otto, A., Simoneit, B.R.T., 2001. Chemosystematics and diagenesis of terpenoids in fossil conifer species and sediment from the Eocene Zeitz formation, Saxony, Germany. Geochim. Cosmochim. Acta 65 (20), 3505–3527.

Otto, A., Simoneit, B.R.T., Rember, W.C., 2005. Conifer and angiosperm biomarkers in clay sediments and fossil plants from the Miocene Clarkia Formation, Idaho, USA. Org. Geochem. 36 (6), 907–922.

Ourisson, G., Albrecht, P., 1992. Hopanoids. 1. Geohopanoids: the most abundant natural products on Earth? Acc. Chem. Res. 25 (9), 398–402.

Pagani, M., Zachos, J.C., Freeman, K.H., Tipple, B., Bohaty, S., 2005. Marked decline in atmospheric carbon dioxide concentrations during the Paleogene. Science 309 (5734), 600–603.

Pagani, M., Pedentchouk, N., Huber, M., Sluijs, A., Schouten, S., Brinkhuis, H., Sinninghe Damste, J.S., Dickens, G.R., Expedition, S., 2006. Arctic hydrology during global warming at the Palaeocene/Eocene thermal maximum. Nature 442 (7103), 671–675.

Pancost, R.D., Sinninghe Damsté, J.S., 2003. Carbon isotopic compositions of prokaryotic lipids as tracers of carbon cycling in diverse settings. Chem. Geol. 195 (1–4), 29–58.

Pancost, R.D., van Geel, B., Baas, M., Damsté, J.S.S., 2000. $\delta^{13}C$ values and radiocarbon dates of microbial biomarkers as tracers for carbon recycling in peat deposits. Geology 28 (7), 663–666.

Pancost, R.D., Baas, M., van Geel, B., Sinninghe Damsté, J.S., 2002. Biomarkers as proxies for plant inputs to peats: an example from a sub-boreal ombrotrophic bog. Org. Geochem. 33 (7), 675–690.

Pancost, R.D., Baas, M., van Geel, B., Sinninghe Damsté, J.S., 2003. Response of an ombrotrophic bog to a regional climate event revealed by macrofossil, molecular and carbon isotopic data. The Holocene 13 (6), 921–932.

Pancost, R.D., Steart, D.S., Handley, L., Collinson, M.E., Hooker, J.J., Scott, A.C., Grassineau, N.V., Glasspool, I.J., 2007. Increased terrestrial methane cycling at the Palaeocene–Eocene thermal maximum. Nature 449 (7160), 332–335.

Pancost, R.D., Taylor, K.W., Inglis, G.N., Kennedy, E.M., Handley, L., Hollis, C.J., Crouch, E.M., Pross, J., Huber, M., Schouten, S., 2013. Early Paleogene evolution of terrestrial climate in the SW Pacific, Southern New Zealand. Geochem. Geophys. Geosyst. 14 (12), 5413–5429.

Pearson, P.N., Palmer, M.R., 2000. Atmospheric carbon dioxide concentrations over the past 60 million years. Nature 406 (6797), 695–699.

Pearson, P.N., van Dongen, B.E., Nicholas, C.J., Pancost, R.D., Schouten, S., Singano, J.M., Wade, B.S., 2007. Stable warm tropical climate through the Eocene epoch. Geology 35 (3), 211–214.

Pearson, P.N., Foster, G.L., Wade, B.S., 2009. Atmospheric carbon dioxide through the Eocene–Oligocene climate transition. Nature 461 (7267), 1110–1113.

Pierrehumbert, R.T., 2002. The hydrologic cycle in deep-time climate problems. Nature 419 (6903), 191–198.

Pocknall, D.T., 1987. Paleoenvironments and Age of the Wasatch Formation (Eocene), Powder River Basin, Wyoming: PALAIOS. v. 2, no. 4, pp. 368–376.

Quirk, M., Wardroper, A., Wheatley, R., Maxwell, J., 1984. Extended hopanoids in peat environments. Chem. Geol. 42 (1), 25–43.

Raghoebarsing, A.A., Smolders, A.J.P., Schmid, M.C., Rijpstra, W.I.C., Wolters-Arts, M., Derksen, J., Jetten, M.S.M., Schouten, S., Sinninghe Damste, J.S., Lamers, L.P.M., Roelofs, J.G.M., Op den Camp, H.J.M., Strous, M., 2005. Methanotrophic symbionts provide carbon for photosynthesis in peat bogs. Nature 436 (7054), 1153–1156.

Riegel, W., Wilde, V., Lenz, O.K., 2012. The Early Eocene of Schöningen (N-Germany) — an interim report. Aust. J. Earth Sci. 105 (1), 88–109.

Robson, B.E., Collinson, M.E., Riegel, W., Wilde, V., Scott, A.C., Pancost, R.D., 2015. Early Paleogene wildfires in peat-forming environments at Schöningen Palaeogeography, Palaeoclimatology, Palaeoecology, Germany, v. 437, pp. 53–62.
Rosa-Putra, S., Nalin, R., Domenach, A.-M., Rohmer, M., 2001. Novel hopanoids from *Frankia* spp. and related soil bacteria. Eur. J. Biochem. 268 (15), 4300–4306.
Ryer, T.A., Langer, A.W., 1980. Thickness change involved in the peat-to-coal transformation for a bituminous coal of Cretaceous age in central Utah. J. Sediment. Res. 50 (3), 987–992.
Scott, A.C., 2002. Coal petrology and the origin of coal macerals: a way ahead? Int. J. Coal Geol. 50 (1), 119–134.
Seifert, W.K., Moldowan, J.M., 1980. The effect of thermal stress on source-rock quality as measured by hopane stereochemistry. Phys. Chem. Earth 12, 229–237.
Simoneit, B.R.T., Grimalt, J.O., Wang, T.G., Cox, R.E., Hatcher, P.G., Nissenbaum, A., 1986. Cyclic terpenoids of contemporary resinous plant detritus and of fossil woods, ambers and coals. Org. Geochem. 10 (4–6), 877–889.
Sinninghe Damsté, J.S., Van Duin, A.C.T., Hollander, D., Kohnen, M.E.L., De Leeuw, J.W., 1995. Early diagenesis of bacteriohopanepolyol derivatives: formation of fossil homohopanoids. Geochim. Cosmochim. Acta 59 (24), 5141–5157.
Sloan, L.C., Pollard, D., 1998. Polar stratospheric clouds: a high latitude warming mechanism in an ancient greenhouse world. Geophys. Res. Lett. 25 (18), 3517–3520.
Sloan, L.C., Walker, J.C., Moore, T., Rea, D.K., Zachos, J.C., 1992. Possible Methane-induced Polar Warming in the Early Eocene.
Slotnick, B.S., Dickens, G.R., Nicolo, M.J., Hollis, C.J., Crampton, J.S., Zachos, J.C., Sluijs, A., 2012. Large-amplitude variations in carbon cycling and terrestrial weathering during the latest Paleocene and earliest Eocene: the record at Mead Stream, New Zealand. J. Geol. 120 (5), 487–505.
Sluijs, A., Brinkhuis, H., 2009. A dynamic climate and ecosystem state during the Paleocene–Eocene Thermal Maximum—inferences from dinoflagellate cyst assemblages at the New Jersey Shelf. Biogeosci. Discuss. 6 (3).
Sluijs, A., Brinkhuis, H., Schouten, S., Bohaty, S.M., John, C.M., Zachos, J.C., Reichart, G.-J., Damsté, J.S.S., Crouch, E.M., Dickens, G.R., 2007. Environmental precursors to rapid light carbon injection at the Palaeocene/Eocene boundary. Nature 450 (7173), 1218–1221.
Stefanova, M., Ivanov, D., Yaneva, N., Marinov, S., Grasset, L., Amblès, A., 2008. Palaeoenvironment assessment of Pliocene Lom lignite (Bulgaria) from bitumen analysis and preparative off line thermochemolysis. Org. Geochem. 39 (11), 1589–1605.
Sýkorová, I., Pickel, W., Christanis, K., Wolf, M., Taylor, G., Flores, D., 2005. Classification of huminite—ICCP System 1994. Int. J. Coal Geol. 62 (1), 85–106.
van Breemen, N., 1995. How *Sphagnum* bogs down other plants. Trends in Ecology & Evolution 10 (7), 270–275.
van Dorselaer, A., Albrecht, P.A., Connan, J., 1975. Changes in composition of polycyclic alkanes by thermal maturation (Yallourn Lignite, Australia). In: Campos, R., Goni, J. (Eds.), Advances in Organic Geochemistry. Enadimsa, Madrid, pp. 53–59.
van Hinsbergen, D.J.J., de Groot, L.V., van Schaik, S.J., Spakman, W., Bijl, P.K., Sluijs, A., Langereis, C.G., Brinkhuis, H., 2015. A Paleolatitude Calculator for Paleoclimate Studies: PLoS ONE. v. 10, no. 6, p. e0126946.
van Winden, J.F., Kip, N., Reichart, G.-J., Jetten, M.S.M., Camp, H.J.M.O.d., Damsté, J.S.S., 2010. Lipids of symbiotic methane-oxidizing bacteria in peat moss studied using stable carbon isotopic labelling. Organic Geochemistry 41 (9), 1040–1044.
van Winden, J.F., Talbot, H.M., De Vleeschouwer, F., Reichart, G.-J., Sinninghe Damsté, J.S., 2012. Variation in methanotroph-related proxies in peat deposits from Misten Bog, Hautes-Fagnes, Belgium. Org. Geochem. 53, 73–79.
Whiticar, M.J., 1999. Carbon and hydrogen isotope systematics of bacterial formation and oxidation of methane. Chem. Geol. 161 (1), 291–314.
Wilson, L.R., Webster, R.M., 1946. Plant microfossils from a Fort Union coal of Montana. Am. J. Bot. 271–278.
Xie, S., Nott, C.J., Avsejs, L.A., Maddy, D., Chambers, F.M., Evershed, R.P., 2004. Molecular and isotopic stratigraphy in an ombrotrophic mire for paleoclimate reconstruction. Geochim. Cosmochim. Acta 68 (13), 2849–2862.
Zheng, Y., Singarayer, J.S., Cheng, P., Yu, X., Liu, Z., Valdes, P.J., Pancost, R.D., 2014. Holocene variations in peatland methane cycling associated with the Asian summer monsoon system. Nat. Commun. 5.